PERFORMANCE ANALYSIS OF AN AOI-AWARE LINK-SELECTION RULE FOR PERIODIC HYBRID FSO/RF STATUS UPDATING UNDER IMPERFECT WEATHER PREDICTION

PHÂN TÍCH HIỆU NĂNG LỰA CHỌN LIÊN KẾT THEO ĐỘ TUỔI THÔNG TIN TRONG HỆ THỐNG FSO/RF CẬP NHẬT TRẠNG THÁI ĐỊNH KỲ VỚI DỰ BÁO KHÔNG HOÀN HẢO

Pham Quang Thai[1,2]*, Hanh Dang-Ngoc[1,2]

[1]*Ho Chi Minh City University of Technology (HCMUT), Vietnam*

[2]*Vietnam National University Ho Chi Minh City (VNU-HCM), Vietnam*

*Corresponding author: pqthai@hcmut.edu.vn

(Received: May 20, 2026; Revised: July 18, 2026; Accepted: July 21, 2026)

DOI: 10.31130/ud-jst.2026.24(7A).356E

Abstract - Status monitoring over hybrid FSO/RF links is governed by data freshness rather than throughput, while common link selection rules usually optimize reliability or capacity. This paper studies periodic status updating over a hybrid FSO/RF link under imperfect binary weather prediction with possibly asymmetric false bad and false good errors. A Markov renewal model is used to capture service quantization, weather evolution, and forecast state correlation, yielding semi analytical average AoI for three schedulers: always RF, always FSO, and forecast following. The results identify an error threshold beyond which forecast following is no longer optimal, especially under high optical availability. The proposed AoI aware selector chooses the lowest AoI policy from model scores. Over 3136 balanced error cases, it matches the best simple policy in over 99% of long period cases and has about 5.8% excess AoI. Additional sweeps examine asymmetric errors, parameter estimation errors, and short source periods.

Key words - Age of Information; hybrid FSO/RF; periodic status updates; link selection; weather prediction

Tóm tắt - Giám sát trạng thái qua FSO/RF lai cần dữ liệu mới hơn thông lượng, trong khi bộ chọn liên kết thường tối ưu độ tin cậy hoặc dung lượng. Bài báo nghiên cứu cập nhật trạng thái định kỳ qua FSO/RF dưới dự báo thời tiết nhị phân không hoàn hảo, có xét sai số false-bad và false-good bất đối xứng. Mô hình Markov-renewal mô tả lượng tử hóa thời gian phục vụ, biến đổi thời tiết và tương quan dự báo–thực tế, từ đó dẫn xuất AoI trung bình bán giải tích cho ba lập lịch: luôn RF, luôn FSO và theo dự báo. Kết quả xác định ngưỡng sai số khiến lập lịch theo dự báo không còn tối ưu, nhất là khi độ sẵn sàng quang cao. Bộ chọn AoI chọn chính sách tốt nhất từ điểm số mô hình. Trên 3136 trường hợp cân bằng sai số, bộ chọn trùng chính sách tốt nhất hơn 99% khi chu kỳ nguồn đủ dài và dư khoảng 5,8% AoI. Khảo sát bổ sung xét độ nhạy với sai số bất đối xứng, ước lượng tham số và chu kỳ nguồn ngắn.

Từ khóa - Độ tuổi thông tin; hệ thống lai FSO/RF; cập nhật trạng thái định kỳ; lựa chọn liên kết; dự báo thời tiết

1. Introduction

Hybrid free-space optical and radio-frequency (FSO/RF) communication combines the high data rate of optical transmission with the weather resilience of an RF backup, making it attractive for backhaul, satellite-ground, and aerial-platform links [1], [2]. Many deployments serve status-monitoring workloads, where a remote source periodically samples an atmospheric, structural, or vehicular process and forwards the latest measurement to a control center. For such workloads, the relevant criterion is freshness rather than throughput. Yet, the hybrid FSO/RF controller switches between modes based on a weather forecast that is rarely perfect, and it remains unclear how forecast unreliability affects status freshness. This paper addresses that gap.

Existing hybrid FSO/RF studies can be grouped into three categories. The first targets physical-layer reliability metrics, including outage probability, ergodic capacity, and bit error rate, under perfect channel knowledge or fixed signal-to-noise-ratio (SNR)-threshold switching [3]–[6]. The second enriches the hybrid architecture with mechanisms such as reconfigurable intelligent surfaces [7], [8], deep reinforcement learning for adaptive mode switching [9], reduced-overhead Markov-chain link selection for space-air-ground integrated networks [10], and proactive optical-availability prediction from RF beacons [11]. The third consists of surveys that consolidate hybrid FSO/RF models and challenges [12], [13]. These studies remain throughput- or reliability-oriented and treat weather forecasts as exact or as binary inputs to fixed switching rules; none analyzes how the Age of Information (AoI) of the resulting status stream depends on forecast quality.

A complementary line of work studies AoI-optimal scheduling. The AoI metric, introduced in [14] and surveyed in [15], [16], measures the time since the most recently received update was generated. AoI-optimal scheduling has been analyzed for single-server queues with controlled sampling [17], energy-harvesting sources [18], multi-source broadcast networks [19], and heterogeneous-channel systems [20]. However, these works assume homogeneous channels or independent service-time distributions and do not capture a hybrid FSO/RF link, in which the faster mode is weather-sensitive, an imperfect binary forecast is observed at each epoch, and a failed optical attempt incurs fallback overhead followed by RF service. Consequently, the natural hybrid FSO/RF rule, forecast-following, which selects FSO whenever the forecast predicts good weather and RF otherwise [3], [5], [21], has not been analyzed for freshness, and no prior work has characterized when its implicit assumption of forecast reliability becomes a liability. Related FSO studies in this journal have analyzed multi-subcarrier transmission and pointing-error effects under Log-Normal turbulence [22], [23].

This paper addresses that gap by analyzing the average AoI of zero-buffer updating over a hybrid FSO/RF link with a two-state weather model and asymmetric false-bad and false-good forecast errors [5], [11], [21]. Within a Markov-renewal framework, we characterize three schedulers-always-RF, always-FSO, and forecast-following-and build an AoI-aware selector that picks the lowest-AoI scheduler from model parameters. The selector is benchmarked against a perfect-information genie that observes the true weather state and solves a dynamic program. The main contributions are:

- We derive semi-analytical average-AoI expressions for always-RF, always-FSO, and forecast-following under periodic updating with imperfect, possibly asymmetric weather prediction, using a Markov-renewal formulation that accounts for service quantization and weather evolution.

- We identify the AoI regime boundary where forecast-following becomes suboptimal and show that the tolerable forecast-error level decreases as optical availability increases.

- We propose a low-complexity AoI-aware selector that chooses the best scheduler from model-derived scores, and we quantify its sensitivity to asymmetric forecast errors, parameter-estimation errors, and the short-period regime.

2. System Model and AoI Analysis

2.1. Hybrid FSO/RF Periodic-Update Model

We consider a point-to-point hybrid link with an FSO mode, which is fast but weather-sensitive, and an RF mode, which is slower but always available. The source generates one fresh status packet every T_s seconds under a periodic zero-buffer replacement rule: at each sampling boundary only the freshest packet is retained. The objective is to minimize the long-run average AoI at the destination.

The FSO link is governed by a two-state continuous-time Markov chain (CTMC) $S(t) \in \{G, B\}$ with transition rates

$$\lambda_{GB} = (1-p_a)\lambda_\Sigma, \quad \lambda_{BG} = p_a\lambda_\Sigma, \tag{1}$$

where $p_a = \Pr[S = G]$ is the stationary good-state probability. The normalized weather-speed parameter is $\eta \triangleq \lambda_\Sigma \mu_R$, where $\mu_R \triangleq \mathbb{E}[T_R]$ is the mean RF service time.

At each decision epoch, the controller receives a one-bit weather forecast $\hat{Y} \in \{\hat{G}, \hat{B}\}$. We distinguish the two forecast-error directions as

$$\varepsilon_G = \Pr[\hat{Y} = \hat{B} | S = G], \quad \varepsilon_B = \Pr[\hat{Y} = \hat{G} | S = B], \tag{2}$$

where $\varepsilon_G, \varepsilon_B \in [0, 0.5)$. Here, ε_G is a false-bad probability that prevents use of a currently good FSO link, whereas ε_B is a false-good probability that triggers an FSO attempt during bad weather. The posterior beliefs are

$$b_{\hat{G}} = \frac{(1-\varepsilon_G)p_a}{(1-\varepsilon_G)p_a + \varepsilon_B(1-p_a)}, \tag{3}$$

$$b_{\hat{B}} = \frac{\varepsilon_G p_a}{\varepsilon_G p_a + (1-\varepsilon_B)(1-p_a)}. \tag{4}$$

When $\varepsilon_G = \varepsilon_B = 0$, the forecast is perfect; when $\varepsilon_G = \varepsilon_B = 1/2$, it is uninformative and $b_{\hat{G}} = b_{\hat{B}} = p_a$. The balanced slice $\varepsilon_G = \varepsilon_B = \varepsilon$ is used later for curve-level interpretation and admits a critical $\varepsilon^\star(p_a, \eta, \theta)$ beyond which forecast-following becomes AoI-suboptimal.

2.2. Service-Time Model

The RF service time is $T_R = L / [W_R \log_2(1+\gamma_R)]$, where γ_R follows a Nakagami-m distribution with shape m and spread Ω, L is the packet size, and W_R is the RF bandwidth. For the FSO mode in state G, the instantaneous SNR is $\gamma_F = \bar{\gamma}_F UV$, where U and V are independent Gamma-Gamma fading factors with parameters (α, β), giving service time $T_F = L / [W_F \log_2(1+\gamma_F)]$. Let $q = \Pr[\gamma_F < \gamma_{\min}]$ denote the direct-outage probability. If FSO fails or the weather state is B, a fallback overhead $d_{\text{fb}} = \kappa\mu_R$ is incurred followed by an independent RF service, where $T_R' \overset{d}{=} T_R$. The state-action service durations are therefore

$$X_{G,F} = \begin{cases} T_F, & \text{w.p. } 1-q, \\ d_{\text{fb}} + T_R', & \text{w.p. } q, \end{cases} \tag{5}$$

$$X_{B,F} = d_{\text{fb}} + T_R', \quad X_{G,R} = X_{B,R} = T_R, \tag{6}$$

with moments $\mu_{s,a} \triangleq \mathbb{E}[X_{s,a}]$ and $\nu_{s,a} \triangleq \mathbb{E}[X_{s,a}^2]$. From (5)–(6), the RF moments are trivially $\mu_{G,R} = \mu_{B,R} = \mu_R$ and $\nu_{G,R} = \nu_{B,R} = \nu_R$, while the FSO effective moments are

$$\mu_{G,F} = (1-q)\mathbb{E}[T_F] + q(d_{\text{fb}} + \mu_R), \tag{7}$$

$$\nu_{G,F} = (1-q)\mathbb{E}[T_F^2] + q(d_{\text{fb}}^2 + 2d_{\text{fb}}\mu_R + \nu_R), \tag{8}$$

$$\mu_{B,F} = d_{\text{fb}} + \mu_R, \quad \nu_{B,F} = d_{\text{fb}}^2 + 2d_{\text{fb}}\mu_R + \nu_R. \tag{9}$$

These moments, together with the parameter set $(p_a, \eta, \varepsilon_G, \varepsilon_B, \theta)$, fully specify the periodic hybrid FSO/RF operating point.

2.3. Periodic AoI Recursion

Define the normalized source period $\theta \triangleq T_s / \mu_R$ and the age index $d_n \in \{1, 2, \ldots\}$, so that the AoI at the start of cycle n is $\Delta_n^- = d_n T_s$. The service overrun in source periods is $J_n = \lceil X_n / T_s \rceil$, giving cycle duration $C_n = J_n T_s$ and the recursion $d_{n+1} = J_n$. During the service interval $[0, X_n]$, the AoI evolves as $\Delta_n^- + t$; upon delivery at time

X_n, the AoI resets to X_n and then grows linearly until the next decision epoch at C_n. The per-cycle AoI area is therefore

$$A_n = \int_0^{X_n} (d_n T_s + t)\mathrm{d}t + \int_{X_n}^{C_n} t\,\mathrm{d}t = d_n T_s X_n + \frac{1}{2}(J_n T_s)^2, \quad (10)$$

and the long-run average AoI under policy π is

$$\bar{\Delta}(\pi) = \frac{\mathbb{E}_\pi[A_n]}{\mathbb{E}_\pi[C_n]}. \quad (11)$$

The expectation is taken under stationary operation of the embedded chain induced by the policy.

2.4. Simple Schedulers and Markov-Renewal Formulation

We consider three simple schedulers: always-RF (π_R), always-FSO (π_F), and forecast-following (π_N), which chooses FSO for $Y = \hat{G}$ and RF for $Y = \hat{B}$. For this policy class, the age recursion $d_{n+1} = J_n$ depends only on the current service duration, hence the transition law does not require additional history, although the pair (d, y) is retained for evaluating the per-cycle AoI area.

For the constant policies, the embedded weather state S_n is the CTMC sampled at the random cycle duration C_n. Over a deterministic cycle of length c,

$$p_{GG}(c) = p_a + (1-p_a)e^{-\lambda_\Sigma c}, \quad (12)$$

$$p_{BG}(c) = p_a(1-e^{-\lambda_\Sigma c}). \quad (13)$$

Under π_R, the service law is identical in both weather states, so the average AoI depends only on the RF moments. Under π_F, the service law differs between G and B through (5)–(6), and the embedded weather distribution is obtained by averaging (12)–(13) over the random cycle duration. For π_N, the action depends on Y_n, which is correlated with S_n through the forecast-error model. Given $Y_n = y$, the posterior weight on state s is $w_y(s)$ from (3)–(4); when $y = \hat{G}$, the controller chooses FSO, and when $y = \hat{B}$, it chooses RF. After each cycle, the weather evolves for duration C_n and a new forecast is drawn.

Under action a, define $J_{s,a} = \lceil X_{s,a} / T_s \rceil$ and $C_{s,a} = J_{s,a} T_s$. The forecast-conditioned expected service time, cycle duration, and squared cycle duration are

$$\bar{\mu}_{y,a} = \sum_s w_y(s)\mu_{s,a}, \quad \bar{c}_{y,a} = \sum_s w_y(s)\mathbb{E}[C_{s,a}], \quad (14)$$

$$\bar{\xi}_{y,a} = \sum_s w_y(s)\mathbb{E}[C_{s,a}^2]. \quad (15)$$

From (10), the expected cycle area from state (d, y) under action a is

$$g(d, y, a) = dT_s\bar{\mu}_{y,a} + \frac{1}{2}\bar{\xi}_{y,a}, \quad (16)$$

with cycle duration $\tau(y, a) = \bar{c}_{y,a}$.

The weather CTMC transitions over the cycle duration (12)–(13), combined with the forecast-error model, determine the next forecast distribution. After a cycle of duration c starting in true state s, the next forecast satisfies $\Pr(Y_{n+1} = \hat{G} \mid S_n = s, C_n = c) = p_{sG}(c)(1-\varepsilon_G) + p_{sB}(c)\varepsilon_B$, yielding a one-step transition kernel

$$\begin{aligned} P^{(p)}_{(d,y)\to(d',y')} = \sum_{s\in\{G,B\}} w_y(s)\mathbb{E}\Big[&\mathbf{1}\{J_{s,a_p(y)} = d'\} \\ &\times \Pr(Y_{n+1} = y' \mid S_n = s, C_{s,a_p(y)})\Big], \end{aligned} \quad (17)$$

where $a_p(y)$ is the action map of policy p. If $\nu^{(p)}(d, y)$ denotes the stationary distribution of the embedded chain, then the average AoI is

$$\bar{\Delta}(\pi_p) = \frac{\sum_{d,y}\nu^{(p)}(d,y)g(d,y,a_p(y))}{\sum_{d,y}\nu^{(p)}(d,y)\tau(y,a_p(y))}. \quad (18)$$

The three policy scores $\Delta_R \triangleq \bar{\Delta}(\pi_R)$, $\Delta_F \triangleq \bar{\Delta}(\pi_F)$, and $\Delta_N \triangleq \bar{\Delta}(\pi_N)$ are evaluated semi-analytically from the system parameters. In practice, $\nu^{(p)}(d, y)$ is obtained from the balance equations of the embedded chain in (17), so the selector is model-based rather than simulation-fitted.

2.5. AoI-Aware Policy Selector

The proposed controller performs policy selection over the simple class $\{\pi_R, \pi_F, \pi_N\}$:

$$\pi_{\text{sel}} = \arg\min_{\pi\in\{\pi_R,\pi_F,\pi_N\}} \bar{\Delta}(\pi). \quad (19)$$

The primary selector uses only $(p_a, \eta, \varepsilon_G, \varepsilon_B, \theta)$ and the service-time moments; it introduces no hand-tuned forecast-error threshold, since all regime boundaries follow from score equalities among Δ_R, Δ_F, and Δ_N. Its cost is solving (17) for each policy, i.e., a small matrix inversion, much lighter than dynamic programming over the full age-forecast state.

For the short-period regime, where the policy scores can be close, we also evaluate a guarded selector. Let $\Delta_{(1)}$ and $\Delta_{(2)}$ denote the smallest and the second-smallest values among $\Delta_R, \Delta_F, \Delta_N$. For $\theta \le 1$, the guarded selector is

$$\pi_g = \begin{cases} \pi_F, & \dfrac{\Delta_{(2)} - \Delta_{(1)}}{\Delta_{(1)}} < \zeta \\ \pi_{\text{sel}}, & \text{otherwise}, \end{cases} \quad (20)$$

with $\zeta = 0.005$. For $\theta > 1$, the guarded selector is not applied.

At moderate-to-high p_a, the dominant transition is between π_N and π_F. In the balanced-error slice, the critical forecast error $\varepsilon^\star$ at which they exchange optimality decreases with p_a: as optical availability grows, the bad-weather state where the forecast adds value becomes rarer, while each false alarm, $Y = \hat{B}$ when $S = G$, wastes a fast optical opportunity by reverting to slow RF. Hence even moderate prediction impairment makes forecast-following AoI-suboptimal when p_a is large. Conversely, at low p_a with near-random forecasts, frequent fallback penalties make always-RF cheapest. The selector captures both transitions as a model-derived design rule.

2.6. Genie Benchmark

To assess proximity to the best achievable freshness, we define a genie benchmark π_{ge} that observes the true weather state and solves the average-cost dynamic program over (d_n, S_n) via relative value iteration. The percentage excess AoI of any policy π is

$$\rho(\pi) = 100 \times \frac{\bar{\Delta}(\pi) - \bar{\Delta}(\pi_{\text{ge}})}{\bar{\Delta}(\pi_{\text{ge}})} \quad (\%). \tag{21}$$

3. Numerical Results

We evaluate the proposed selector over the full sweep $p_a \in \{0.2, \ldots, 0.9\}$, $\eta \in \{0.03, 0.1, 0.3, 1, 3, 10, 30\}$, $\varepsilon \in \{0, 0.05, \ldots, 0.49\}$, and $\theta \in \{0.5, 1, \ldots, 15\}$, totaling 3136 operating points. The parameter values used below lie within ranges commonly adopted in the hybrid FSO/RF literature, and are summarized as follows. The FSO channel uses Gamma-Gamma fading with parameters $(\alpha, \beta) = (4.0, 1.9)$, average SNR $\bar{\gamma}_F = 20$ dB, and bandwidth $W_F = 50$ MHz, corresponding to a moderate-turbulence regime representative of hybrid FSO/RF studies in [1], [3], [5]. The RF channel uses Nakagami-m fading with $m = 2$, $\Omega = 15$ dB, and bandwidth $W_R = 10$ MHz, representative of a line-of-sight microwave or millimeter-wave backup link [3], [4]. The status-packet size $L = 1000$ bits is a standard value for AoI-driven status updates [14], [15], and the baseline fallback factor $\kappa = 0.3$ reflects a moderate protocol-level switching overhead consistent with prior hybrid FSO/RF link-switching designs [2], [10]; sensitivity to κ is examined separately in Table 3. Each Monte Carlo point uses 250 trials of 4000 cycles with 250 burn-in. The selector is computed from the semi-analytical scores in Section 2, while Monte Carlo validates the resulting decisions.

Table 1 validates the asymmetric-error extension before focusing on the balanced-error slice. Across the tested $(\varepsilon_G, \varepsilon_B)$ pairs, the selector matches the best-simple policy in at least 91.3% of operating points, with mean AoI gaps below 102 ns and 95th-percentile gaps below 455 ns. These results indicate that the selector remains effective when false-bad and false-good errors are unequal. The following figures therefore use $\varepsilon_G = \varepsilon_B = \varepsilon$ to isolate the effect of overall forecast reliability without adding forecast-bias direction.

Table 1. *Sensitivity to asymmetric forecast errors. Each row aggregates 392 operating points over p_a, η, and θ. Gaps are relative to the best simple policy*

ε_G	ε_B	**Match (%)**	**Mean gap (ns)**	**95th gap (ns)**
0.1	0.1	96.2	39.0	0.0
0.1	0.3	94.6	33.0	20.5
0.2	0.2	94.6	101.4	15.6
0.2	0.4	91.3	78.4	454.7
0.3	0.1	93.6	69.2	237.4
0.3	0.3	95.2	53.9	0.0
0.4	0.2	92.3	89.7	283.0

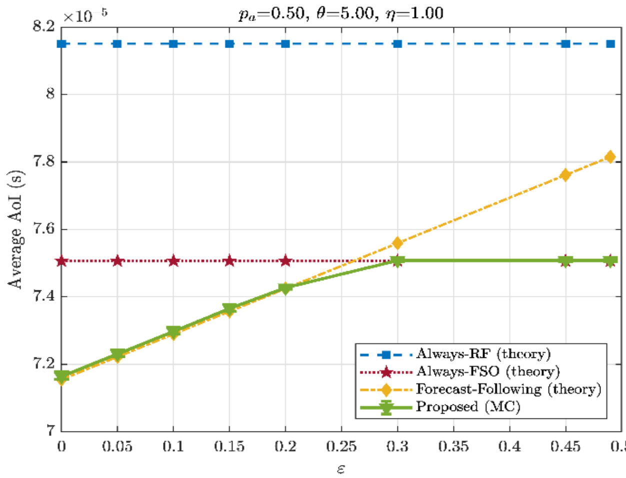

Figure 1. *Average AoI versus balanced forecast error ε with $\varepsilon_G = \varepsilon_B = \varepsilon$ at $p_a = 0.5$, $\theta = 5$, $\eta = 1$. Solid lines: semi-analytical AoI of simple policies. Markers: Monte Carlo proposed selector with 95% CIs*

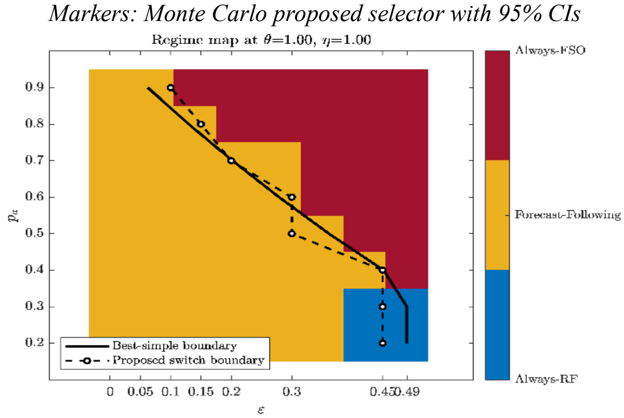

Figure 2. *Best-simple-policy regime map over the balanced-error (ε, p_a) plane at $\theta = 1$, $\eta = 1$. Solid line: AoI-best-simple boundary. Dashed line: proposed selector boundary*

Figures 1 and 2 show the main policy-crossover behavior under balanced forecast errors. In Figure 1, forecast-following is best when $\varepsilon = 0$ but becomes worse than always-FSO near $\varepsilon \approx 0.26$ as the forecast becomes less reliable. The proposed selector follows the lower envelope of the three simple policies and switches to always-FSO by $\varepsilon = 0.30$, confirming that the model-based scores capture the crossover. Figure 2 further shows that the critical error $\varepsilon^\star$ decreases as p_a increases, from about

0.45 at $p_a = 0.4$ to about 0.06 at $p_a = 0.9$. This trend is expected because, when optical availability is high, false-bad predictions more often waste fast FSO opportunities. The selector matches the best simple policy at 54 of 64 grid points, with mismatches mainly near regime boundaries and in the low-p_a, high-ε region.

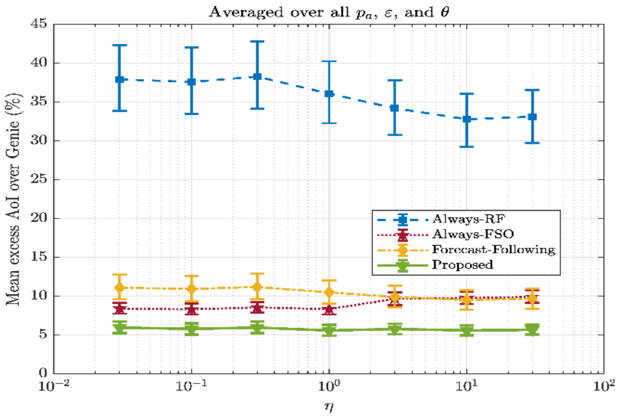

Figure 3. *Mean excess AoI $\rho(\pi)$ relative to the genie benchmark versus η, averaged over all p_a, balanced ε, and θ. Each point aggregates 448 operating conditions*

Figure 3 shows that the selector remains close to the genie benchmark across weather timescales. Always-RF incurs about 33–36% excess AoI, while always-FSO and forecast-following stay around 9–11%. The proposed selector reduces this to 5.6–5.9%, approximately halving the gap to the genie relative to forecast-following. Quantitatively, it reduces the mean excess AoI by about 41–46% relative to forecast-following and 31–43% relative to always-FSO. Its nearly flat curve over η also indicates that weather timescale is not the dominant source of selector loss in the tested model.

Table 2. *Selector match rate (%) and mean AoI gap to the best simple policy, grouped by θ and η. Guarded columns are evaluated only for $\theta \le 1$ and aggregate over all η. Each cell aggregates over all p_a and balanced ε*

θ	Match rate (%)			Mean gap (ns)			Guarded match (%)	Guarded gap (ns)
	$\eta<1$	$\eta=1$	$\eta>1$	$\eta<1$	$\eta=1$	$\eta>1$		
0.5	62.5	62.5	80.2	990	760	180	90.0	133.5
1	90.6	90.6	87.5	140	140	240	92.6	62.5
2–3	96.9	98.4	97.7	8.9	4.4	3.9	–	–
≥ 5	99.5	99.5	99.3	0.52	0.82	0.48	–	–

Table 2 localizes the main residual loss to the short-period regime, especially $\theta = 0.5$, where service-time quantization makes policy ranking difficult and small score differences can change the selected policy. As θ increases, this quantization effect weakens and the selector rapidly becomes near-exact: for $\theta \ge 5$, the match rate exceeds 99% with sub-ns mean gaps. The guarded variant in (20) directly addresses the short-period limitation by avoiding overly sensitive decisions when the two best policy scores are nearly tied. It improves the aggregate short-period match rate to 90.0% at $\theta = 0.5$ and 92.6% at $\theta = 1$, while also reducing the corresponding mean gaps.

Table 3. *Sensitivity to the fallback factor κ, evaluated over the full 3136-point sweep for each tested value. Mean and 95th-percentile AoI gaps are relative to the best simple policy; FSO-use and RF-use fractions are averaged over all cycles of the proposed selector*

κ	Match (%)	Mean gap (ns)	95th gap (ns)	FSO use (%)	RF use (%)
0.1	93.0	62.6	156	79.3	20.7
0.3	93.2	115.4	291	68.8	31.2
0.5	92.3	144.3	651	62.0	38.0

Tables 3 and 4 summarize practical robustness from two complementary perspectives. Table 3 shows that increasing κ makes fallback more costly and therefore shifts the selector toward RF use; nevertheless, the selector does not collapse into an all-RF rule, and the match rate remains between 92.3% and 93.2%, with mean gaps below 145 ns. Table 4 further tests whether the selector remains reliable when the model parameters used for scoring are imperfect. The largest impact comes from errors in p_a and the false-bad probability ε_G, because both affect the perceived availability of fast FSO opportunities. By contrast, perturbing RF and FSO service-time moments produces much smaller gaps. Even under the largest tested perturbations, the mean AoI gap remains below 187 ns for probability estimates and below 56 ns for service-time moment estimates.

Table 4. *Sensitivity to parameter-estimation errors. The physical system uses the true parameters, while the selector scores are computed from the perturbed estimates. Each row aggregates the full 3136-point balanced-error sweep*

Perturbed estimate	Error	Match (%)	Mean gap (ns)	95th gap (ns)
none	0	95.6	51.6	0.0
p_a	±0.05	89.2–93.4	57.1–97.1	244.5–457.3
p_a	±0.10	84.6–88.0	115.6–186.9	744.9–1297.8
ε_G	±0.05	90.1–91.1	73.6–90.7	369.3–529.2
ε_G	±0.10	82.6–86.4	123.8–185.4	862.2–1219.4
ε_B	±0.05	95.0–95.6	47.4–60.3	0.0–3.2
ε_B	±0.10	93.0–95.4	47.4–69.4	0.0–232.2
RF moments	±10%	95.4–95.6	48.7–55.4	0.0
	±20%	95.5–96.1	42.3–48.3	0.0
FSO moments	±10%	95.5–95.6	49.9–52.3	0.0
	±20%	95.6–95.6	49.5–51.6	0.0

Overall, the selector captures the AoI regime boundary, remains stable under asymmetric forecast errors and fallback variation, and is most sensitive to errors that change perceived FSO availability.

4. Conclusion

This paper analyzed periodic status updating over a hybrid FSO/RF link with imperfect binary weather prediction, including asymmetric forecast errors. Using a Markov-renewal formulation, we characterized the average AoI of always-RF, always-FSO, and forecast-following schedulers, and showed that forecast-following becomes suboptimal when forecast errors exceed a critical threshold, especially under high optical availability. The proposed AoI-aware selector matches the AoI-best simple policy in over 99% of operating points when θ is at least 5 and achieves about 5.8% mean excess AoI relative to the perfect-information genie across 3136 tested conditions.

The residual loss mainly occurs in the short-period regime due to stronger service-time quantization; a guarded short-period variant gives a modest reduction in the mean gap for $\theta \le 1$. Future work may consider richer turbulence and pointing-error conditions [12], multi-state forecasts, and learning-based scheduling over broader policy spaces [9]. Overall, the results suggest that periodic hybrid FSO/RF updating can achieve near-best freshness by selecting an interpretable scheduler from optical availability, forecast quality, and source period.

Acknowledgments: We acknowledge Ho Chi Minh City University of Technology (HCMUT), VNU-HCM for supporting this study.

REFERENCES

[1] M. A. Khalighi and M. Uysal, "Survey on free space optical communication: A communication theory perspective," *IEEE Commun. Surveys Tuts.*, vol. 16, no. 4, pp. 2231–2258, 2014.

[2] W. Zhang, S. Hranilovic, and C. Shi, "Soft-switching hybrid FSO/RF links using short-length Raptor codes: Design and implementation," *IEEE J. Sel. Areas Commun.*, vol. 27, no. 9, pp. 1698–1708, Dec. 2009.

[3] T. Rakia, H.-C. Yang, M.-S. Alouini, and F. Gebali, "Outage analysis of practical FSO/RF hybrid system with adaptive combining," *IEEE Commun. Lett.*, vol. 19, no. 8, pp. 1366–1369, Aug. 2015.

[4] B. Makki, T. Svensson, M. Brandt-Pearce, and M.-S. Alouini, "On the performance of millimeter wave-based RF-FSO multi-hop and mesh networks," *IEEE Trans. Wireless Commun.*, vol. 16, no. 12, pp. 7746–7759, Dec. 2017.

[5] H. Kazemi, M. Uysal, and F. Touati, "Outage analysis of hybrid FSO/RF systems based on finite-state Markov chain modeling," in *Proc. 3rd Int. Workshop Opt. Wireless Commun. (IWOW)*, Sep. 2014, pp. 11–15.

[6] S. Sharma, A. S. Madhukumar, and R. Swaminathan, "Switching-based cooperative decode-and-forward relaying for hybrid FSO/RF networks," *J. Opt. Commun. Netw.*, vol. 11, no. 6, pp. 267–281, May 2019.

[7] Y. He, W. Qi, P. Shen, and L. Lu, "Performance analysis of RIS-aided hybrid RF-FSO communications with index modulation," *IEEE Photon. J.*, vol. 17, no. 3, pp. 1–17, Jun. 2025.

[8] D. Kim, H. S. Park, and B. C. Jung, "Performance analysis of RIS-assisted dual-hop mixed FSO-RF UAV communication systems," *Digit. Commun. Netw.*, vol. 11, no. 4, pp. 1271–1279, Aug. 2025.

[9] S. Henna, A. A. Minhas, M. S. Khan, and M. S. Iqbal, "Ensemble consensus representation deep reinforcement learning for hybrid FSO/RF communication systems," *Opt. Commun.*, vol. 530, p. 129186, Mar. 2023.

[10] P. S. Bithas, H. E. Nistazakis, A. Katsis, and L. Yang, "Hybrid FSO/RF communications in space-air-ground integrated networks: A reduced overhead link selection policy," *Electronics*, vol. 13, no. 4, p. 806, Feb. 2024.

[11] M. Ibrahim *et al.*, "Anticipating optical availability in hybrid RF/FSO links using RF beacons and deep learning," *IEEE Trans. Mach. Learn. Commun. Netw.*, vol. 2, pp. 1369–1388, 2024.

[12] H. Hassan, S. Althunibat, A. Al-Mbaideen, M. O. Hasna, and K. A. Qaraqe, "A survey on hybrid free space optical and radio frequency systems: Classification, progress, observations, and challenges," *IEEE Access*, vol. 13, pp. 63994–64060, 2025.

[13] S. Phuchortham and H. Sabit, "A survey on free-space optical communication with RF backup: Models, simulations, experience, machine learning, challenges and future directions," *Sensors*, vol. 25, no. 11, p. 3310, May 2025.

[14] S. Kaul, R. Yates, and M. Gruteser, "Real-time status: How often should one update?" in *Proc. IEEE INFOCOM*, Mar. 2012, pp. 2731–2735.

[15] R. D. Yates, Y. Sun, D. R. Brown, S. K. Kaul, E. Modiano, and S. Ulukus, "Age of information: An introduction and survey," *IEEE J. Sel. Areas Commun.*, vol. 39, no. 5, pp. 1183–1210, May 2021.

[16] A. Kosta, N. Pappas, and V. Angelakis, "Age of information: A new concept, metric, and tool," *Found. Trends Netw.*, vol. 12, no. 3, pp. 162–259, Nov. 2017.

[17] Y. Sun, E. Uysal-Biyikoglu, R. D. Yates, C. E. Koksal, and N. B. Shroff, "Update or wait: How to keep your data fresh," *IEEE Trans. Inf. Theory*, vol. 63, no. 11, pp. 7492–7508, Nov. 2017.

[18] R. D. Yates, "Lazy is timely: Status updates by an energy harvesting source," in *Proc. IEEE Int. Symp. Inf. Theory (ISIT)*, Jun. 2015, pp. 3008–3012.

[19] I. Kadota, A. Sinha, E. Uysal-Biyikoglu, R. Singh, and E. Modiano, "Scheduling policies for minimizing age of information in broadcast wireless networks," *IEEE/ACM Trans. Netw.*, vol. 26, no. 6, pp. 2637–2650, Dec. 2018.

[20] A. Maatouk, S. Kriouile, M. Assad, and A. Ephremides, "On the optimality of the Whittle's index policy for minimizing the age of information," *IEEE Trans. Wireless Commun.*, vol. 20, no. 2, pp. 1263–1277, Feb. 2021.

[21] J. Tóth, Ľ. Ovsenik, J. Turán, L. Michaeli, and M. Márton, "Classification prediction analysis of RSSI parameter in hard switching process for FSO/RF systems," *Meas.*, vol. 116, pp. 602–610, Feb. 2018.

[22] P. Q. Vuong *et al.*, "Performance investigating of a multi-subcarrier free space optic using log-normal channel model," *The University of Danang - Journal of Science and Technology*, vol. 23, no. 2, pp. 59–64, Feb. 2025, doi: 10.31130/ud-jst.2025.474E.

[23] D. H. Ai, D. T. Tuan, and H. D. Trung, "Pointing error effects on performance of amplify-and-forward relaying fso systems using sc-qam signals over gamma-gamma atmospheric turbulence channels". *The University of Danang - Journal of Science and Technology*, vol. 6, no. 103, pp. 1–5, Jun. 2016.